

Fine structure of the morphotropic phase boundaries of

$\text{PbZr}_{1-x}\text{Ti}_x\text{O}_3$, $\text{Pb}(\text{Mg}_{1/3}\text{Nb}_{2/3})_{1-x}\text{Ti}_x\text{O}_3$, and

$\text{Pb}(\text{Zn}_{1/3}\text{Nb}_{2/3})_{1-x}\text{Ti}_x\text{O}_3$.

A twelfth-order Landau-type treatment.

I. A. Sergienko* and Yu. M. Gufan

Institute of Physics, Rostov State University, Rostov-on-Don, 344104, Russia

S. Urazhdin

Department of Physics and Astronomy,

Michigan State University, East Lansing, MI 48824

Abstract

Recently discovered fine structure of the morphotropic phase boundaries in highly piezoelectric mixture compounds of Pb-based oxides shows the importance of anharmonic interactions in these systems. An adequate Landau-type description of the ferroelectric phase transitions in these compounds is achieved by use of a twelfth-order expansion of the nonequilibrium potential in terms of the phenomenological order parameter. The theory describes both PZT and PZN- x PT types of phase diagrams, including the newly found monoclinic and orthorhombic phases. Evolution of both polarization and lattice parameters with temperature and composition is calculated in good agreement with experiment. Anomalously large piezoelectric coefficients are predicted in the vicinity of the phase transition lines.

PACS numbers: 77.80.Bh, 77.84.Dy, 81.30.Dz, 77.65.Bn

I. INTRODUCTION

For many years, perovskite-type materials have been a subject of extensive research in both experimental and theoretical physics. On one hand, different representatives of the perovskite family exhibit a host of physical phenomena, such as piezoelectricity, ferroelectricity, and superconductivity; on the other hand, perovskite structure is a relatively simple and, thus, attractive object for theoretical studies.

Even though there is a long history of studies of perovskites, they still present new surprises. Recent X-ray and neutron diffraction studies on solid solutions $\text{PbZr}_{1-x}\text{Ti}_x\text{O}_3$ (PZT), $\text{Pb}(\text{Mg}_{1/3}\text{Nb}_{2/3})_{1-x}\text{Ti}_x\text{O}_3$ (PMN- x PT), and $\text{Pb}(\text{Zn}_{1/3}\text{Nb}_{2/3})_{1-x}\text{Ti}_x\text{O}_3$ (PZN- x PT)^{1,2,3,4,5} have revealed new phases in the vicinity of the morphotropic phase boundary⁶ on the $T-x$ phase diagram of the solutions. In a narrow Ti concentration range ($x = 46 - 52\%$), the low temperature structure of PZT was found to be monoclinic M_A with polarization vector \mathbf{P} directed along $[uvw]$, $u < v$ pseudo-cubic direction³. A similar M_A structure has also been recently seen in PMN- x PT below room temperature for $x = 35\%$ ⁵. Another fine structure of the morphotropic phase boundary has been found in PZN- x PT. For $x = 9 - 11\%$, the low-temperature structure is orthorhombic with $\mathbf{P} \parallel [101]$ ⁴. Rhombohedral unpoled crystal of PZN-8%PT was also found to exhibit irreversible monoclinic M_C ($\mathbf{P} \parallel [0uv]$) distortion when an electric field above a certain critical value is applied along the $[001]$ pseudo-cubic direction⁷.

Early theoretical investigations of phase transitions in perovskites were concentrated on BaTiO_3 , which goes through a sequence of phases upon cooling: cubic(C), tetragonal(T), orthorhombic(O), and rhombohedral(R). Devonshire⁸ explains the behavior of BaTiO_3 within the framework of a phenomenological Landau-type expansion up to sixth order in terms of the ferroelectric order parameter – polarization \mathbf{P} . While successfully describing the phase diagram of BaTiO_3 , the potential used in Ref. 8 lacks the high-order terms necessary to describe highly anharmonic systems. Using a geometric argument based on Curie principle, Zheludev and Shuvalov⁹ classified possible positions of \mathbf{P} with respect to the cubic unit cell. Due to the purely symmetric nature of this approach, it fails to distinguish between monoclinic phases M_A and M_B ($\mathbf{P} \parallel [uvw]$, $u > v$), because these phases have the same crystallographic symmetry Cm . The group-theoretical relationship between the geometric method and Landau approach was established in Ref. 10. It was shown that the limitations

of the phenomenological model arising from the potential truncation at finite-order terms can be removed by use of the rational basis of integrity. A proper expansion in terms of the rational basis of integrity describes general properties of the phases and transitions between them. Using this approach, Gufan and Sakhnenko¹¹ found that on a two-dimensional (say, $T - x$) phase diagram of perovskites there can be a point (T_0, x_0) where five phases C, R, O, M_C , and T co-exist. They calculated the phase diagram in the vicinity of this five-phase point. Only small solutions of the equations of state that are close to the five-phase point were considered, justifying expansion in powers of small parameters $(T - T_0), (x - x_0)$. However, the results of this work do not apply to the recently discovered phases of the mixture compounds of Pb-based complex oxides. In this case, the R-O-T and R- M_A -T triple points are separate from the C-R-T triple point, invalidating the N -phase point approximation. Therefore, theoretical consideration cannot be limited to small solutions of the equations of state, especially for the lowest symmetry phases.

*Ab initio*¹², as well as phenomenological, calculations¹³, have been used to account for the presence of monoclinic phases on the $T - x$ phase diagrams of ferroelectric perovskites. Vanderbilt and Cohen¹³ calculate the phase diagram in the space of phenomenological parameters within the framework of Landau-Devonshire theory. Their model is based on the eighth-order expansion of the Landau potential in terms of \mathbf{P} , with a fixed absolute value of spontaneous polarization \mathbf{P}_s . Although monoclinic phases appear in the phase diagram of the model, it does not incorporate cubic and triclinic (Tri) phases. It also cannot describe the experimental temperature dependence of the physical properties, such as lattice constants, because the polarization value is fixed.

Having considered a number of successively more complicated models, a natural question arises: What is the most general phenomenological model of the phase diagram of a cubic system induced by a ferroelectric order parameter? By a group-theoretical argument, if the basis of integrity of invariants formed by the order parameter components contains polynomials of maximal order n , then at least a $2n$ -th-order phenomenological model is necessary to describe all the possible phases induced by the order parameter¹⁴. This statement is true for the irreducible representations of groups generated by reflections, including the $Pm3m$ symmetry of the perovskite structure. We will show that, in the case of perovskites, the Landau potential has to be expanded up to the twelfth-order terms to describe the phase diagram induced by the ferroelectric order parameter. The results of the analysis of a twelfth-order

model are presented in this paper. In our approach, the polarization value also is determined self-consistently from the equations of state, thus avoiding the mentioned limitations of the previous studies. In Sec. II, we present the solutions resulting in a phase diagram containing all the phases allowed by the symmetry of the ferroelectric order parameter. In Sec. III, we fit the $T - x$ phase diagrams of PZT and PZN-PT, and also calculate temperature and concentration dependence of the lattice parameters and spontaneous polarization. In Sec. IV, we discuss the piezoelectric properties of the compounds in the vicinity of the newly found phase boundaries.

II. TWELFTH-ORDER LANDAU-TYPE MODEL

Three algebraically independent $Pm3m$ -invariant polynomials can be formed from the polarization vector components (P_x, P_y, P_z) .

$$\begin{aligned} J_1 &= P_x^2 + P_y^2 + P_z^2, \\ J_2 &= P_x^2 P_y^2 + P_y^2 P_z^2 + P_x^2 P_z^2, \\ J_3 &= P_x^2 P_y^2 P_z^2. \end{aligned} \tag{1}$$

The ferroelectric part of the Landau potential can then be expressed in terms of algebraic combinations of J_1, J_2 , and J_3 . Since polynomials of up to sixth order are present in the rational basis of integrity (1), the nonequilibrium potential has to be expanded up to the twelfth order terms:

$$\begin{aligned} F^{(fe)} = & a_1 J_1 + a_2 J_1^2 + b_1 J_2 && - \text{2nd and 4th order terms} \\ & + a_3 J_1^3 + d_{12} J_1 J_2 + c_1 J_3 && - \text{6th order terms} \\ & + a_4 J_1^4 + d_{112} J_1^2 J_2 + b_2 J_2^2 + d_{13} J_1 J_3 && - \text{8th order terms} \\ & + a_5 J_1^5 + d_{1112} J_1^3 J_2 + d_{122} J_1 J_2^2 + d_{113} J_1^2 J_3 + d_{23} J_2 J_3 && - \text{10th order terms} \\ & + a_6 J_1^6 + d_{11112} J_1^4 J_2 + d_{1122} J_1^2 J_2^2 + b_3 J_2^3 + d_{1113} J_1^3 J_3 && \left. \vphantom{F^{(fe)}} \right\} - \text{12th order terms} \\ & + d_{123} J_1 J_2 J_3 + c_2 J_3^2 && \end{aligned} \tag{2}$$

A complete investigation of extrema of the function $F^{(fe)}(\mathbf{P})$ in the multi-dimensional parameter space is a rather tedious exercise. However, main features of the phase diagram can be obtained from simplified models based on potential (2) with some terms omitted.

The truncated potential should satisfy at least two requirements: i) it has to be bounded from below, and ii) it should be structurally stable in catastrophe theory sense^{14,15}. The latter requirement provides that small perturbations, which can arise from the omitted in (2) terms, do not drastically change the results obtained in a simplified model. In the Appendix, we briefly describe how compliance with the second requirement can be verified.

A twelfth-order model

$$F_{init}^{(fe)} = a_1 J_1 + b_1 J_2 + c_1 J_3 + a_2 J_1^2 + b_2 J_2^2 + c_2 J_3^2 \quad (3)$$

meets both requirements when a_2, b_2 , and c_2 are positive quantities, while a_1, b_1 , and c_1 are parameters driving phase transitions, and can be of any sign. In spite of its simplicity, model (3) is in full agreement with the results of the group-theoretical analysis of the ferroelectric phase transitions in perovskites. It gives an account of all the phases C, T, O, R, M_A , M_B , M_C , and Tri, and it correctly describes the phase boundaries. For example, although the symmetry groups of the phases $M_A(M_B)$ and R obey a group-subgroup relation $Cm \subset R3m$, phase transitions R- M_A and R- M_B , as described by the model (3), cannot be of second order¹³.

A complete phase diagram of the Landau potential (3) can be constructed in the space of phenomenological parameters (a_1, b_1, c_1) . All the characteristic features can be seen from the two-dimensional cross-sections in the $a_1 b_1$ plane, as shown in Fig. 1.

Below we show how the phase diagram of Fig. 1 was analytically obtained, using the example of phase R. Minimizing the potential (3) with respect to P_x, P_y, P_z , and then imposing the condition $P_x = P_y = P_z = P_s/\sqrt{3}$, we obtain the value of spontaneous polarization P_s as a solution of the equation of state

$$a_1 + \frac{2}{3}(3a_2 + b_1)P_s^2 + \frac{c_1}{9}P_s^4 + \frac{4b_2}{9}P_s^6 + \frac{2c_2}{243}P_s^{10} = 0, \quad (4)$$

which obeys the stability conditions

$$(3a_2 + b_1) + \frac{c_1}{3}P_s^2 + 2b_2P_s^4 + \frac{5c_2}{81}P_s^8 \geq 0, \quad (5)$$

$$b_1 + \frac{c_1}{3}P_s^2 + \frac{2}{3}b_2P_s^4 + \frac{2c_2}{81}P_s^8 \leq 0. \quad (6)$$

The parametric equations for the boundaries of the phase stability domain are obtained by replacing the inequality in either (5) or (6) with an equality and solving it together with

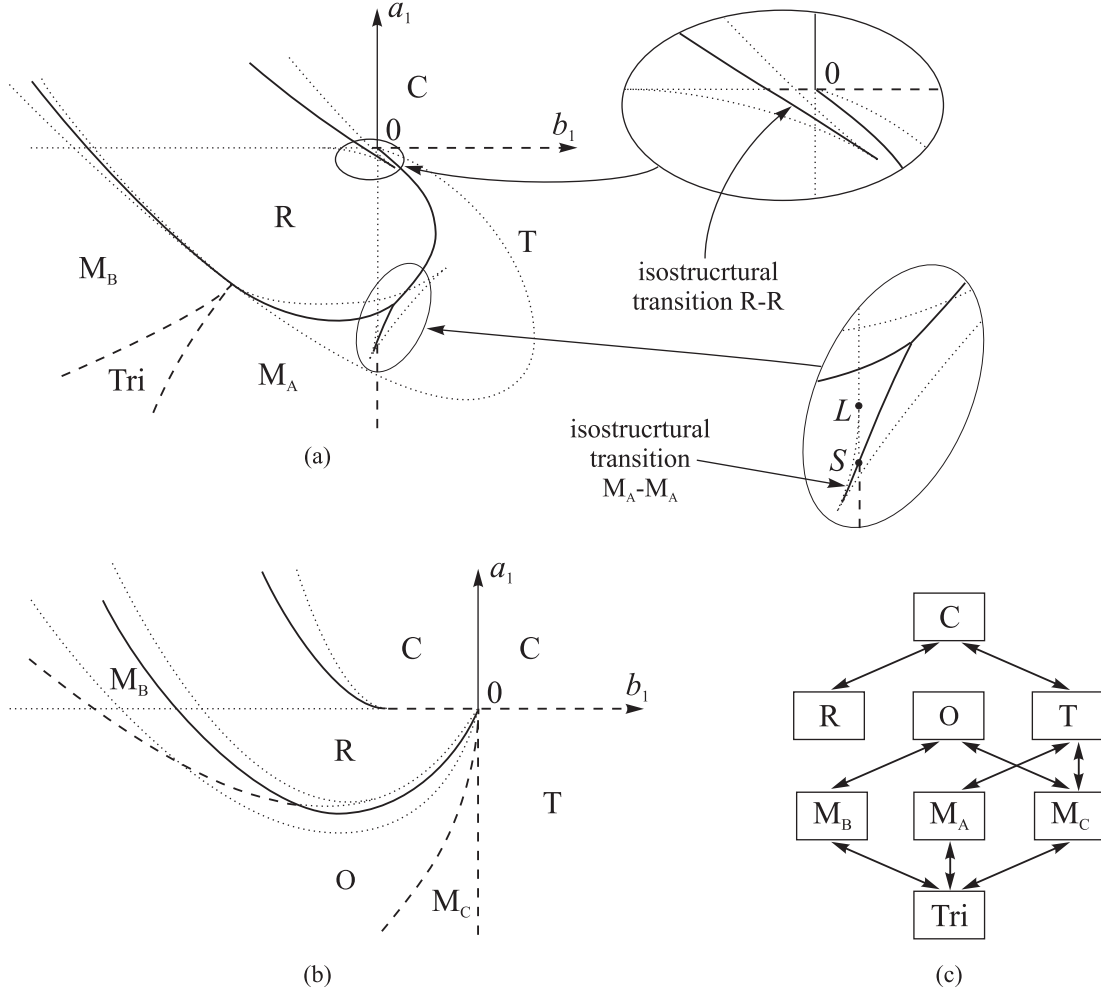


FIG. 1: (a), (b) Phase diagram in (a_1, b_1) plane for the potential $F_{init}^{(fe)}$ for $c_1 < 0$ (a) and $c_1 > 0$ (b). Solid lines – first-order phase boundaries; dashed lines – second-order phase boundaries; dotted lines – stability boundaries of phases. (c) Diagram of possible second-order phase transitions between the phases.

(4). The line resulting from (4) and (5) has a cusp at $c_1 < 0$ shown in the top inset of Fig. 1(a). This feature is defined by the parametric equation

$$c_1 + 12b_2P_{cusp}^2 + \frac{20c_2}{27}P_{cusp}^6 = 0 \quad (7)$$

This equation has no real solutions for $c_1 > 0$, as the cusp merges with the a_1 axis. Another interesting feature of the phase diagram is a first-order transition line below the b_1 axis, shown in the top inset of Fig. 1(a). It corresponds to an *isostructural* transition between two phases with the same structure and symmetry R, with the value of P_s being the only

difference between them¹⁶. A similar transition line appears in phase M_A and is shown enlarged in the bottom inset.

All possible second-order phase transitions are shown in Fig. 1(c). In agreement with the general analysis¹¹, only phases R and T are accessible from phase C via a second-order transition. The M_C -Tri second order transition occurs in the $c_1 = 0$ plane and is not shown in Fig. 1.

We would like to point out some other important features of the phase diagram of Fig. 1, which can be represented in a simple analytical form. For $c_1 > 0$, phase M_C lies between T- M_C and O- M_C second-order phase boundaries defined respectively by

$$b_1 = 0, \text{ and } b_1 = -\frac{a_1^2 b_2}{8a_2^2}. \quad (8)$$

The second-order O- M_B transition line is parabolic in the (a_1, b_1) parameter space

$$(2b_2 a_1 + c_1 b_1)^2 - (c_1^2 + 8a_2 b_2)(c_1 a_1 - 4a_2 b_1) = 0. \quad (9)$$

The lowest symmetry Tri phase appears at $c_1 < 0$ between phases M_A and M_B in a slice restricted by a parametrically defined line

$$\begin{cases} a_1(t) = -4a_2 t^2 + \frac{c_1 a_2}{c_2 t^4}, \\ b_1(t) = -2b_2 t^4 + \frac{2c_1 b_2}{c_2 t^2}, \end{cases} \quad (10)$$

where t is a parameter. The coordinates of the four-phase R- M_B - M_A -Tri critical point can be obtained from (10):

$$a_1 = 3a_2 \left(\frac{4c_1}{c_2} \right)^{1/3}; \quad b_1 = -3b_2 \left(\frac{2c_1^2}{c_2^2} \right)^{1/3}. \quad (11)$$

In Sec. III we will give special attention to some other features of the phase diagram shown in the lower inset of Fig. 1(a). They are related to the fine structure of the phase diagram, recently observed in PZT^{3,4} and PMN- x PT⁵.

III. PHASE DIAGRAMS, LATTICE PARAMETERS AND POLARIZATION

The seemingly simple twelfth-order model potential $F_{init}^{(fe)}$ (3) has led, as can be seen from Fig. 1, to a complex phase diagram describing all eight phases allowed by the symmetry

of the problem. All possible second-order phase transitions among the proper ferroelectric phases in perovskites are established by Fig. 1(c), so any approximations made to describe transitions driven by the ferroelectric order parameter should not add or forbid any second-order transition lines obtained in the model (3). On the other hand, first-order phase transitions between any two of the eight phases can be expected, since, in general, there are no arguments that can forbid these transitions. For example, a direct O–T transition has been experimentally observed in PZN- x PT⁷ and earlier in BaTiO₃.

In Fig. 2 we plot the experimental phase diagrams of PZT and PZN- x PT together with our calculations based on the model described. In Sec. II we have shown that the triple point of phases R, T, and M_A can appear as an intersection of the first-order phase transition lines (see Fig. 1(a)). A second-order phase transition M_A–T is possible below the critical point S . This is exactly the topological structure of the T–M_A phase transition line that has been observed in PZT³. To obtain reasonable agreement with the experiment, we assumed that the coefficients a_1 and b_1 in (3) are linear functions of temperature and composition, while the rest of the parameters are constant:

$$\begin{aligned} a_1 &= \alpha_T(T - T_0) + \alpha_x(x - x_0), \\ b_1 &= \beta_T(T - T_0) + \beta_x(x - x_0). \end{aligned} \tag{12}$$

Keeping in mind the global topology of the phase diagram shown in Fig. 1, we can identify the features related to the perovskite compounds. When applying the developed model to the particular systems, we add some symmetry allowed terms to the expansion (3). This enables us to use simple temperature and concentration dependencies of the phenomenological parameters while achieving a good fit to the experimental phase diagrams. To model a PZT-type phase diagram (also related to PMN- x PT), we use an expansion for the potential

$$F_{PZT}^{(fe)} = F_{init}^{(fe)} + d_{12}J_1J_2. \tag{13}$$

Upon this modification, the T–M_A second-order transition line remains straight:

$$b_1 = \frac{d_{12}a_1}{2a_2}. \tag{14}$$

Since the phenomenological phase diagram can always be isomorphically transformed to fit the experimental data, we do not try to obtain a perfect quantitative fit. Rather, we

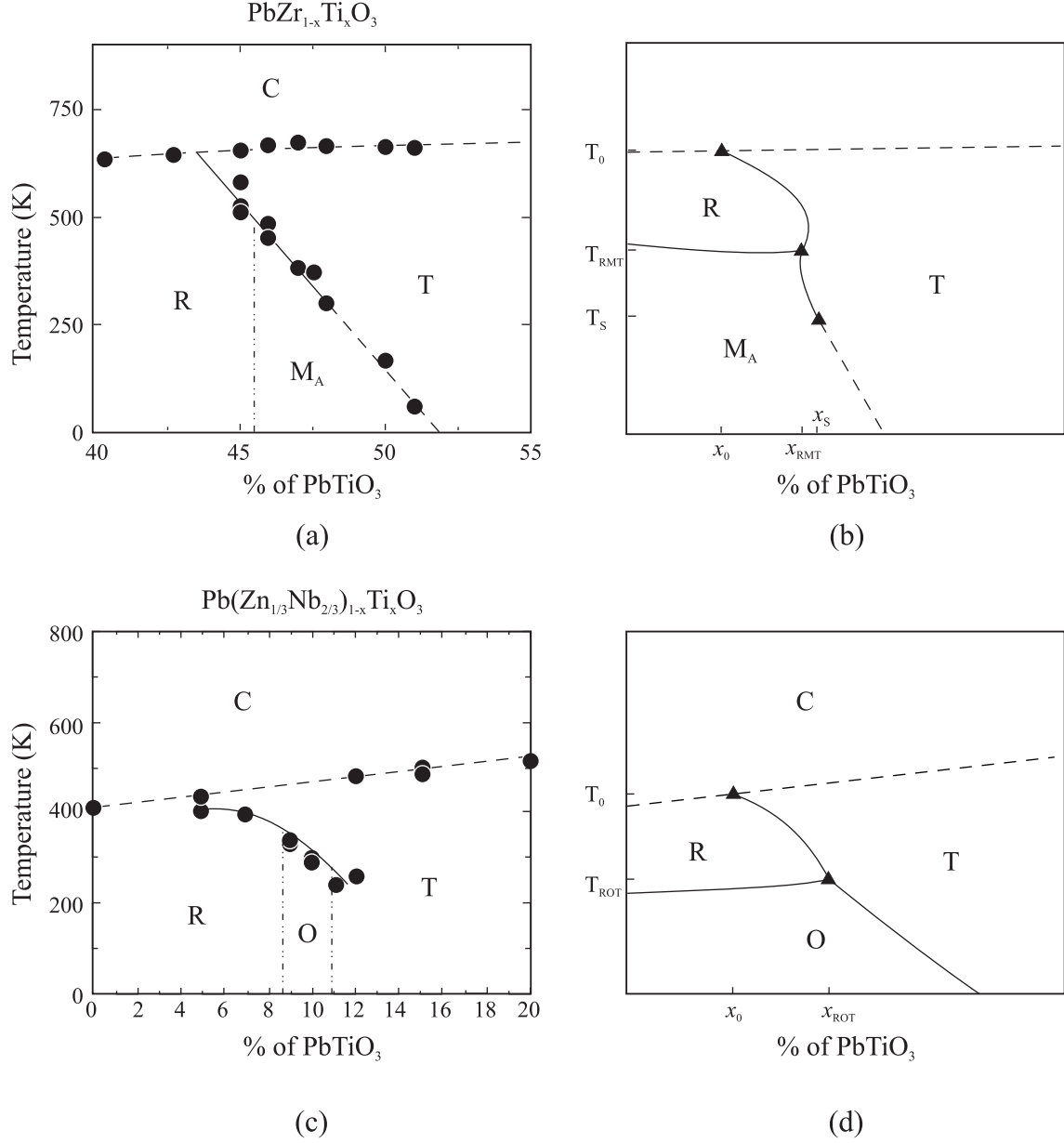


FIG. 2: (a), (c) Phase diagrams of PZT and PZN- x PT from Refs. 3,4,6,17. (b), (d) Phase diagrams calculated based on the model potentials $F_{\text{PZT}}^{(fe)}$ and $F_{\text{PZN}}^{(fe)}$, as described in the text. Critical points are shown as triangles, their coordinates are marked on axes.

calculate the coefficients in arbitrary units to reproduce the qualitative features of the phase diagram. The calculated values for PZT are

$$\begin{aligned} c_1 &= -25, \quad a_2 = 9, \quad b_2 = 0.8, \quad d_{12} = -0.3, \\ c_2 &= 3.6, \quad \alpha_T = 1, \quad \alpha_x = -0.07, \quad \beta_T = 0.05, \quad \beta_x = 1. \end{aligned} \quad (15)$$

We used a relatively large absolute value for c_1 to obtain comparable lengths of the

first-order M_A -T transition line and R-T phase boundary, as seen in the experiment. This results in a vanishingly small region of coexistence of the two isostructural M_A phases (see the bottom inset in Fig. 1(a)). The critical point S then almost merges with point L , the latter being a tangency point of the T- M_A second-order transition line continuation and the stability boundary of phase M_A .

For the expansion (13), point L has coordinates:

$$a_1 = \frac{2a_2^2 c_1}{4a_2 b_2 - d_{12}^2}, \quad b_1 = \frac{a_2 c_1 d_{12}}{4a_2 b_2 - d_{12}^2}. \quad (16)$$

More extensive modifications of $F_{init}^{(fe)}$ have been used to accommodate the features of the experimental phase diagram of PZN- x PT, namely a direct O-T transition and, more importantly, the separation of the triple points R-O-T and C-R-T:

$$F_{PZN}^{(fe)} = F_{init}^{(fe)} + d_{12} J_1 J_2 + d_{13} J_1 J_3. \quad (17)$$

We find that the part of the global phase diagram, relevant to PZN- x PT, is almost unaffected by the variation of c_2 . Therefore, we assume $c_2 = 0$. The other coefficients are

$$\begin{aligned} c_1 &= -40, \quad a_2 = 9, \quad b_2 = 0.7, \quad d_{12} = 8, \quad d_{13} = 13, \\ \alpha_T &= 1, \quad \alpha_x = -0.8, \quad \beta_T = 0.6, \quad \beta_x = 1. \end{aligned} \quad (18)$$

Variation of the lattice constants with external conditions can be taken into account by introducing an elastic part of the nonequilibrium Landau potential:

$$\begin{aligned} F^{(el)} &= \gamma_1(P_x^2 + P_y^2 + P_z^2)(e_{xx} + e_{yy} + e_{zz}) + \gamma_2[(P_x^2 + P_y^2)e_{zz} + (P_y^2 + P_z^2)e_{xx} + (P_x^2 + P_z^2)e_{yy}] \\ &\quad + \gamma_3(P_x P_y e_{xy} + P_y P_z e_{yz} + P_x P_z e_{xz}) + \lambda_1(e_{xx}^2 + e_{yy}^2 + e_{zz}^2) \\ &\quad + \lambda_2(e_{xx} e_{yy} + e_{yy} e_{zz} + e_{xx} e_{zz}) + \lambda_3(e_{xy}^2 + e_{yz}^2 + e_{xz}^2), \end{aligned} \quad (19)$$

where e_{ik} are the strain tensor components. Thermal expansion effects are disregarded in (19). Spontaneous values of the strain tensor components are obtained by minimizing $F^{(el)}$ with respect to e_{ik} . Following this procedure, we find the lattice parameters as a function of the polarization. For example, the rhombohedral lattice constants a_r and α_r can be expressed in terms of the cubic lattice parameter a_c and the rhombohedral spontaneous

polarization P_s :

$$\begin{aligned}\frac{a_r - a_c}{a_c} &= -\frac{3\gamma_1 + 2\gamma_2}{6(\lambda_1 + \lambda_2)} P_s^2, \\ \cos \alpha_r &= -\frac{\gamma_3}{3\lambda_3} P_s^2.\end{aligned}\tag{20}$$

We calculate temperature evolution of the lattice parameters and polarization in a number of phases for various compositions, as well as composition dependencies for a fixed temperature (Fig. 3). Experimental curves can be found in Refs. 1,2,7. Truncation of $F^{(el)}$ at the second-order terms is justified by the experimental fact that distortions of the cubic cell are small, less than 5% for both PZT³ and PZN- x PT⁴. The corresponding small parameters that appear in the theory are γ_i/λ_k for all i and k . We assume for both PZT and PZN- x PT

$$\lambda_1 = \lambda_2 = \lambda_3 = 1,\tag{21}$$

and take the coefficients of the elastic-ferroelectric interaction terms to be

$$\gamma_1 = \gamma_2 = 0.03, \quad \gamma_3 = -0.025\tag{22}$$

for PZT, and

$$\gamma_1 = -0.01, \quad \gamma_2 = 0.02, \quad \gamma_3 = -0.006\tag{23}$$

for PZN- x PT.

IV. PIEZOELECTRIC PROPERTIES

The components of the piezoelectric tensor \mathbf{d}_{ik} can also be deduced from the potentials $F_{PZT}^{(fe)} + F^{(el)}$ and $F_{PZN}^{(fe)} + F^{(el)}$. They are inversely proportional to combinations of the second derivatives of $F_{PZT}^{(fe)}$ and $F_{PZN}^{(fe)}$ with respect to P_x, P_y, P_z . Some of these combinations vanish at the stability boundaries of the phases, resulting in anomalous values of the piezoelectric constants.

For each phase on the phase diagrams Fig. 2, we find the components \mathbf{d}_{ik} which can be large, working in the pseudo-cubic orthogonal basis. In the R phase, all four independent piezoelectric constants are expected to be large at all the phase transition lines with phases T, M_A , and O. Especially strong piezoelectric properties can be found at the phase transition

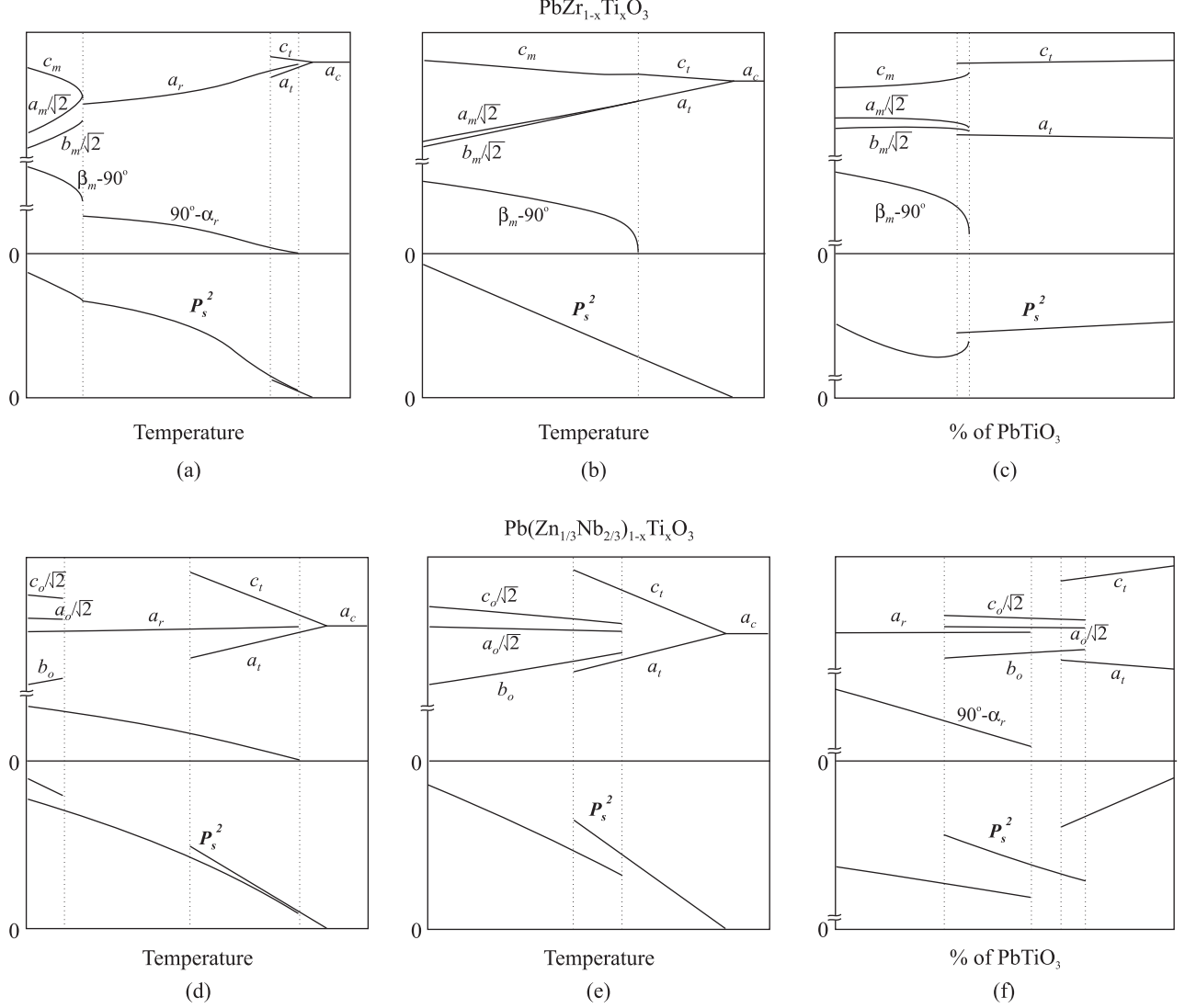


FIG. 3: Evolution of the lattice parameters and \mathbf{P}_s^2 with (a), (b), (d), (e) temperature (fixed x), and (c), (f) Ti content (fixed T), calculated for the potential $F_{PZT}^{(fe)} + F^{(el)}$: (a) $x_0 < x < x_{RMT}$, (b) $x > x_S$, (c) $T_{RMT} < T < T_S$ and for the potential $F_{PZN}^{(fe)} + F^{(el)}$: (d) $x_0 < x < x_{ROT}$, (e) $x > x_{ROT}$, (f) $T < T_{ROT}$. Dotted lines are a guide for the eye.

lines that are close to the stability boundaries. As seen from Fig. 3(a), this is just the case for the R- M_A phase boundary where a possible hysteresis is very small.

The tetragonal piezoelectric \mathbf{d}_{15} component of the piezoelectric tensor can be large at the T-R, T- M_A and T-O phase boundaries, while \mathbf{d}_{33} and \mathbf{d}_{31} are not expected to have anomalies in temperature and composition dependence at these lines.

A complex behavior of the piezoelectric constants is expected in phase M_A at the bound-

ary with phase T. In the second-order transition part of this phase boundary, no anomalies are expected. This is because no stability condition is violated there, even though it is a bifurcation line where the monoclinic solution of the equations of state becomes imaginary. However, this situation changes drastically when M_A -T is a first-order phase transition. In this part of the M_A -T boundary and at the M_A -R boundary, all ten monoclinic piezoelectric coefficients can be large.

Another verifiable prediction of our theory is the connection between the proximity of phase M_A to the triclinic distortion and anomalies in the monoclinic piezoelectric coefficients d_{11} , d_{12} , d_{14} , and d_{15} , at low temperatures.

Finally, d_{33} and d_{31} can be large in phase O at the T boundary, and d_{24} – at the R boundary.

V. CONCLUSION

We have shown that the increasingly high-order phenomenological models, used to describe the highly anharmonic systems PZT, PMN- x PT and PZN- x PT, are approximations to the complete twelfth-order model (2). Such a complex potential is difficult to analyze, but even the significantly simplified models $F_{PZT}^{(fe)} + F^{(el)}$ and $F_{PZN}^{(fe)} + F^{(el)}$ describe the phase diagram of the compounds reasonably well. We use these model potentials to classify the phase boundaries, as well as to calculate the evolution of the lattice constants with temperature and Ti concentration, and obtain good agreement with the experiment. In particular, the model reproduces the separation of the triple points R-O-T and R- M_A -T from the C-R-T triple point, and the switching of the M_A -T phase transition between the first- and the second-order types. We also predict an anomalous behavior of certain piezoelectric constants along the phase transition lines. These predictions elucidate the nature of the ultra-high piezoelectricity and make our theory easily verifiable.

*

APPENDIX A: STRUCTURAL STABILITY OF PHENOMENOLOGICAL POTENTIALS

In this appendix we review the method based on catastrophe theory, which is used to analyze the stability of the potential functions.

Let p be the dimensionality of the representation driving phase transitions, and m - the number of invariants, constituting the integrity basis formed from the functions of this representation. In general, $m \geq p$, and there exist $m - p$ syzygies - algebraic relations of higher than first order among the m invariant polynomials. We consider the simplest case of an irreducible representation of a group generated by reflections, for which $m = p$. This is the situation for the ferroelectric order parameter in $Pm3m$ group, as seen from Eq. (1).

To determine the structural stability of some potential function $F(J_1, \dots, J_m)$, we need to introduce the algebraic combinations:

$$U_i(J_1, \dots, J_m) = \sum_{k=1}^m \frac{\partial F}{\partial J_k} (\nabla J_k, \nabla J_i), i = 1, \dots, m, \quad (\text{A1})$$

where ∇J_i is the gradient of invariant J_i in the order parameter space. Scalar products that appear in (A1) can always be expressed in terms of invariant polynomials J_1, \dots, J_m . An omitted in the potential function term can not violate the type of the extremal behavior of the potential function if its coefficient is small and the term can be written as

$$\sum_{i=1}^m \mathcal{P}_i(J_1, \dots, J_m) U_i(J_1, \dots, J_m) + \text{h. o. t.} \quad (\text{A2})$$

Here $\mathcal{P}_i(J_1, \dots, J_m)$ are some polynomials and ‘h. o. t.’ stands for ‘higher order terms’.

Following this algorithm, we obtain for the integrity basis (1) and potential (3)

$$\begin{aligned} (\nabla J_1)^2 &= 4J_1, & (\nabla J_1, \nabla J_2) &= 8J_2, \\ (\nabla J_2)^2 &= 4J_1J_2 + 12J_3, & (\nabla J_2, \nabla J_3) &= 8J_1J_3, \\ (\nabla J_3)^2 &= 4J_2J_3, & (\nabla J_1, \nabla J_3) &= 12J_3. \end{aligned} \quad (\text{A3})$$

and

$$\begin{aligned} U_1 &= 4a_1J_1 + \text{h. o. t.} \\ U_2 &= 8a_1J_2 + \text{h. o. t.} \\ U_3 &= 12a_1J_3 + \text{h. o. t.} \end{aligned} \quad (\text{A4})$$

It is now clear that every term in (2), additional to (3), can be represented in the form (A2). However, there is another restriction that arises from the requirement for a model to produce all the phases allowed by the symmetry of the order parameter. As can be seen from Eq. (10), triclinic phase cannot appear in the phase diagram of the truncated below the twelfth-order Landau potential expansion (3). Consequently, the potential (3) is the simplest model that meets all the requirements mentioned above.

* E-mail:iserg@uic.rsu.ru

- ¹ B. Noheda, J. A. Gonzalo, A. C. Caballero, C. Moure, D. E. Cox, and G. Shirane, Appl. Phys. Lett. **74**, 2059 (1999).
- ² B. Noheda, J. A. Gonzalo, L. E. Cross, R. Guo, S.-E. Park, D. E. Cox, and G. Shirane, Phys. Rev. B **61**, 8687 (2000).
- ³ B. Noheda, D. E. Cox, G. Shirane, R. Guo, B. Jones, and L. E. Cross, Phys. Rev. B **63**, 14103 (2001).
- ⁴ D. La-Orauttapong, B. Noheda, Z.-G. Ye, P.M. Gehring, J. Toulouse, D. E. Cox, and G. Shirane, (submitted); cond-mat/0108264.
- ⁵ Z.-G. Ye, B. Noheda, M. Dong, D. Cox, and G. Shirane, Phys. Rev. B, **64**, (2001) (to be published); cond-mat/0107276.
- ⁶ B.Jaffe, W. R. Cook, H. Jaffe, *Piezoelectric Ceramics* (Academic Press, London, 1971).
- ⁷ B. Noheda, D. E. Cox, G. Shirane, S.-E. Park, L. E. Cross, and Z. Zhong, Phys. Rev. Lett. **86**, 3891 (2001).
- ⁸ A.F. Devonshire, Phil. Mag. **40**, 1040 (1949); Phil. Mag. **42**, 1065 (1951); Adv. Phys. **3**, 85 (1954).
- ⁹ I. S. Zheludev and L. A. Shuvalov, Kristallografiya **1**, 681 (1956), (in Russian).
- ¹⁰ Yu. M. Gufan, Fiz. Tverd. Tela **13**, 225 (1971) [Sov. Phys. Solid State **13**, 175 (1971)].
- ¹¹ Yu. M. Gufan and V. P. Sakhnenko, Zh. Eksp. Teor. Fiz. **69**, 1429 (1975) [Sov. Phys. JETP **42**, 728 (1975)].
- ¹² L. Bellaiche, A. Garcia, and D. Vanderbilt, Phys. Rev. Lett. **84**, 5427 (2000).
- ¹³ D. Vanderbilt and M. H. Cohen, Phys. Rev. B **63**, 94108 (2001).
- ¹⁴ A. M. Prokhorov, Yu. M. Gufan, E. S. Larin, E. G. Rudashevski, and V. B. Shirokov, Dokl.

- Akad. Nauk SSSR **277**, 1369 (1984), [Sov. Phys. Dokl.] **29**, 656 (1984).
- ¹⁵ V. I. Arnold, A. N. Varchenko, S. M. Gusein-Zade, *Singularities of Differentiable Maps. The Classification of Critical points, Caustics and Wave Fronts*, edited by V.I. Arnold (Birkhäuser, 1985).
- ¹⁶ Yu. M. Gufan and E. S. Larin, Dokl. Akad. Nauk SSSR **242 (6)**, 1311 (1978) [Sov. Phys. Dokl. **23(10)**, 754 (1978)].
- ¹⁷ J. Kuwata, K. Uchino, and S. Nomura, *Ferroelectrics* **37**, 579 (1981).
- ¹⁸ R. Guo, L.E. Cross, S-E. Park, B. Noheda, D.E. Cox, and G. Shirane, *Phys. Rev. Lett.* **84**, 5423 (2000).